DIGITAL COMPENSATION OF THE THRUST VECTOR CONTROL SYSTEMS

PREPARED BY

SAMPLED-DATA CONTROL SYSTEMS GROUP
AUBURN UNIVERSITY

C. L. PHILLIPS, TECHNICAL DIRECTOR

TECHNICAL REPORT
NOVEMBER 13, 1964

CONTRACT NAS8-11274

GEORGE C. MARSHALL SPACE FLIGHT CENTER

NATIONAL AERONAUTICS AND SPACE ADMINISTRATION

HUNTSVILLE, ALABAMA 35812

APPROVED BY

C. M. Weaver
Head Professor
Electrical Engineering

SUBMITTED BY

H. M. Sumner
Project Leader

TABLE OF CONTENTS

LIST OF SYMBOLS

W_{ss} = Control engine transfer function

H_o = Zero order hold

D = Digital compensator transfer function

β_e = Continuous control engine deflection angle, degrees

β_e^* = Sampled control engine deflection angle, degrees

T = Sampling period, seconds

ω_s = Sampling frequency, radians per second

G_1 = Transfer function in attitude channel

G_2 = Transfer function in attitude rate channel

R = System input

β_c = Engine command signal

ϕ_R = Attitude error

$\dot{\phi}_R$ = Attitude rate

LIST OF FIGURES

FORWARD

This report is a technical summary of the progress made by the Electrical Engineering Department, Auburn University, toward fulfillment of Contract No. NAS8-11274 granted to Auburn Research Foundation, Auburn, Alabama. The contract was awarded May 28, 1964, by the George C. Marshall Space Flight Center, National Aeronautics and Space Administration, Huntsville, Alabama.

SUMMARY

The pulsed transfer function of the simplified thrust vector control system for a Saturn-type vehicle is derived. An example is worked for the digital compensation of an unstable control system, with the compensation in the attitude error channel. The problem of compensation in other channels is not considered. Also the effect of the compensation on the dynamic response is not considered.

PERSONNEL

The following named staff members of Auburn University have actively participated on this project:

C. H. Weaver	Head Professor Department of Electrical Engineering
H. M. Summer	Professor of Electrical Engineering
G. T. Nichols	Associate Professor of Electrical Engineering
C. L. Phillips	Associate Professor of Electrical Engineering
C. L. Rogers	Assistant Professor of Electrical Engineering
J. S. Boland	Graduate Assistant in Electrical Engineering
D. W. Kelly	Graduate Assistant in Electrical Engineering

DIGITAL COMPENSATION OF THE THRUST VECTOR CONTROL SYSTEM

C. L. Phillips, J. S. Boland, and D. W. Kelly

I. INTRODUCTION

The purpose of this study is to determine methods of stability analysis and digital compensation of a thrust vector control system for a Saturn-type vehicle. Digital compensation is to be employed in the attitude error channel. In this study, no additional compensation is to be used. The complete control system consists of the control engine transfer function, W_{cs}, in the forward path with attitude error, attitude rate, and lateral acceleration feedback loops. For this study, the vehicle is assumed to be a rigid body and the lateral acceleration feedback loop is omitted.

The steps involved in the analysis of the simplified system are:

1. Derivation of the equations for the sampled output and for the continuous output of the control system, assuming an input in the attitude error channel.
2. Stability analysis of the uncompensated sampled-data system and the uncompensated continuous-data system, by use of the Nyquist diagram.
3. Determination of a digital compensator transfer function which will stabilize the system, by use of the Nyquist diagram.
4. Determination of an equivalent continuous-data transfer function which will stabilize the continuous-data system.

II. ANALYSIS OF THE SIMPLIFIED THRUST VECTOR CONTROL SYSTEM WITH DIGITAL COMPENSATION

For the simplified thrust vector control system shown in Figure 1,

$$W_{cs}(s) = \frac{\beta_e(s)}{\beta_c(s)}$$

$$G_1(s) = \frac{\beta_s(s)}{\beta_c(s)}$$

$$G_2(s) = \frac{\beta_s(s)}{\beta_e(s)}$$

The block H_o represents a zero-order hold, and has the transfer function

$$H_o(s) = \frac{1-e^{-sT}}{s} = \frac{1-z^{-1}}{s} \qquad (1)$$

The block D represents a digital compensator which has the transfer function

$$D(z) = \frac{a_o + a_1 z^{-1} + \cdots + a_n z^{-n}}{b_o + b_1 z^{-1} + \cdots + b_m z^{-m}} \qquad (2)$$

The realizability conditions on D(z) are that all coefficients are real, and that $b_o \neq 0$.[1]

Since the input, r(t), to the system is sampled before being operated upon by a continuous part of the circuit, a transfer function independent of the input can be found for this system. However, if the input were operated upon by a continuous part of the system, G(s), before being sampled, the output of the sampler would be $(RG)^*$, where the asterisk indicates the Laplace transform of the sampled function and where

$$(RG)^* \neq R^*G^*$$

Thus the input function could not be factored from the output of the sampler, and a transfer function independent of the input could not be written.

For Figure 1,

$$\beta_c = G_2\beta_e + H_oD^*(R^* + \phi_R^*) \tag{3}$$

Also

$$\beta_e = W_{ss}\beta_c = W_{ss}G_2\beta_e + W_{ss}H_oD^*(R^* + \phi_R^*) \tag{4}$$

Note that $\phi_R^* = (G_1\beta_e)^*$, but β_e^* cannot be factored from ϕ_R^*.

Solving (4) for β_e in terms of R^* and ϕ_R^*,

$$\beta_e = \frac{W_{ss} H_o}{1-W_{ss}G_2} D^*(R^* + \phi_R^*) \tag{5}$$

Since $\phi_R = G_1\beta_e$, then, from (5),

$$\phi_R = \frac{W_{ss}G_1H_o}{1-W_{ss}G_2} D^* (R^* + \phi_R^*) \tag{6}$$

In order to express ϕ_R as a function of only the input and the system parameters, it is necessary to take the pulse transform of (6). Then the terms due to ϕ_R can be expressed as a single term, ϕ_R^*. Thus

$$\phi_R^* = \left(\frac{W_{ss}G_1H_o}{1-W_{ss}G_2}\right)^* D^*(R^* + \phi_R^*) \tag{7}$$

and therefore

$$\phi_R^* = \frac{\left(\frac{W_{ss}G_1H_o}{1-W_{ss}G_2}\right)^* D^* R^*}{1 - \left(\frac{W_{ss}G_1H_o}{1-W_{ss}G_2}\right)^* D^*} \tag{8}$$

Substituting (8) into (6),

$$\phi_R = \frac{\left(\frac{W_{ss}G_1H_o}{1-W_{ss}G_2}\right) D^* R^*}{1 - \left(\frac{W_{ss}G_1H_o}{1-W_{ss}G_2}\right)^* D^*} \tag{9}$$

Since $\beta_e = \phi_R/G_1$,

$$\frac{\beta_e}{R^*} = \frac{\left(\frac{W_{ss}H_o}{1 - W_{ss}G_2}\right) D^*}{1 - \left(\frac{W_{ss}G_1H_o}{1 - W_{ss}G_2}\right)^* D^*} \tag{10}$$

Equation (10) is entirely a function of s, but contains the term e^{sT}. Thus, in general, a pole-zero type of analysis cannot be used with (10). A discussion of the methods of analysis of this equation is given in Appendix B. Appendix A is the derivation of (10) and (11) by signal flow graphs. The usual method of analysis of (10) is to take the pulse transform of β_e. Then

$$\frac{\beta_e^*}{R^*} = \frac{\left(\frac{W_{ss}H_o}{1 - W_{ss}(G_2)}\right)^* D^*}{1 - \left(\frac{W_{ss}G_1H_o}{1 - W_{ss}(G_2)}\right)^* D^*} \tag{11}$$

If the substitution $e^{sT} = z$ is made in (11), the z-transformed transfer function is

$$\frac{\beta_e(z)}{R(z)} = \frac{\left(\frac{W_{ss}H_o}{1 - W_{ss}G_2}\right)(z)D(z)}{1 - \left(\frac{W_{ss}G_1H_o}{1 - W_{ss}G_2}\right)(z)D(z)} \tag{12}$$

The methods of analysis used in continuous-data systems, i.e., Nyquist diagram, root locus, etc., can now be applied to (12) in the z-plane. However, through the transformation $z = e^{sT}$, the $j\omega$ axis in the s-plane transforms into the unit circle in the z-plane. Thus, in the z-plane, the unit circle separates the stable region for roots (the interior of the unit circle) from the unstable region for roots.

III. STABILITY ANALYSIS OF UNCOMPENSATED CONTINUOUS-DATA SYSTEM AND UNCOMPENSATED SAMPLED-DATA SYSTEM

Consider first the sampled-data system as shown in Figure 1. The z-transformed closed-loop transfer function is given by (12). For the case without compensation, (12) can be modified to

$$\frac{\beta_o(z)}{R(z)} = \frac{\left(\frac{W_{ss}H_o}{1 - W_{ss}G_2}\right)(z)}{1 - \left(\frac{W_{ss}G_1H_o}{1 - W_{ss}G_2}\right)(z)} \tag{13}$$

A numerical example will now be worked which investigates the stability of (13) by its Nyquist diagram. Let

$$F_1(z) = -\left(\frac{W_{ss}G_1H_o}{1 - W_{ss}G_2}\right)(z) \tag{14}$$

Then

$$F_1(s) = \frac{0.9407\,(1 - e^{sT})}{s(s^4 + 25s^3 + 624.97027s^2 + 0.19745s - 18.58125)} \tag{15}$$

when the functions used for the example are

$$W_{ss}(s) = \frac{1}{s^2 + 25s + 625}$$

$$G_1(s) = \frac{-0.94068468}{s^2 - 0.02972784}$$

$$H_o(s) = \frac{1 - \varepsilon^{-sT}}{s}$$

$$G_2(s) = \frac{-0.94068468s}{s^2 - 0.02972784}$$

The constants in $G_1(s)$ and $G_2(s)$ listed above are time varying and are given here as the typical values during the 40th second of flight.

Expanding (15) in a partial fraction expression

$$F_1(s) = (1 - \varepsilon^{-sT}) \left[\frac{-0.050626303}{s} + \frac{0.025249055}{s - 0.17167813} + \frac{0.025377247}{s + 0.17318333} \right. \tag{16}$$

$$\left. + \frac{(2.0239777 + j13.905322)\times 10^{-9}}{s + 12.499247 + j21.650201} + \frac{(2.0239777 - j13.905322)\times 10^{-9}}{s + 12.499247 - j21.650201} \right]$$

The sampling frequency is 25 cps and the sampling period, T, is 0.04 seconds. Given these values, the z-transform of (16) is

$$F_1(z) = \frac{0.0000116z^3 - 0.0000097z^2 + 0.0000352z - 0.0000118}{(z - 1.00689076)(z - 0.99309661)(z^2 - 0.78593283z + 0.36790159)} \tag{17}$$

The Nyquist path in the z-plane can be obtained by letting z vary from 1 + j0 to - 1 + j0 along the upper half of the unit circle. This corresponds to varying the frequency, ω, in the s plane from 0 to $+\infty$. As is the case in the s-plane, there is no need to consider the path in the lower half of the z-plane because mirror symmetry is obtained in the F(z)-plane about the real axis.

The Nyquist plot of (17), shown as Curve A in Figure 3, was obtained using the digital computer program given in Appendix III. Because of the wide range of variations in the magnitude of $F_1(z)$, the Nyquist is shown as a plot of magnitude in db versus phase in degrees. The magnitude is normalized to - 160 db. The stability of the system can be determined by investigating the number of encirclements about the zero db point.

From Nyquist theory, the following must hold true:

$$N = Z - P \tag{18}$$

where P is the number of poles of the open loop transfer function outside the unit circle, Z is the number of zeroes of the characteristic equation of the closed loop system outside the unit circle, and N is the number of clockwise encirclements of the zero db point when the contour around the unit circle in the z-plane is taken counterclockwise. From (17), P is determined to be one. The Nyquist diagram in Figure 3, Curve A, shows no encirclements of the zero db point, indicating that N is zero. Therefore, for (18) to be true, Z must be one and the system is unstable.

The transfer function for the continuous-data, uncompensated system can be obtained from (10) or from Figure 2.

$$\frac{\beta_e}{R} = \frac{\dfrac{W_{ss}}{1 - G_2 W_{ss}}}{1 - \dfrac{G_1 W_{ss}}{1 - G_2 W_{ss}}} \tag{19}$$

If (19) is simplified, the following is obtained:

$$\frac{\beta_e}{R} = \frac{W_{ss}}{1 - W_{ss}(G_1 + G_2)} \tag{20}$$

which could have been written directly from Figure 2 by inspection. In order to get a better comparison between the sampled-data and continuous-data Nyquist diagrams, however, the denominator of (19) will be investigated.

Substituting the values of the transfer functions given above into (19) and simplifying

$$-\left(\frac{G_1 W_{ss}}{1 - G_2 W_{ss}}\right)(s) = \frac{0.940681\overline{63}}{s^4+25s^3+624.97027s^2+0.19745s-18.58125} \qquad (21)$$

The Nyquist plot of (21) is shown as Curve C of Figure 3.

In the low frequency range, the Nyquist diagram of the continuous-data system approximates the Nyquist diagram of the sampled-data system if the sampling frequency is high, and if the effects of the zero-order hold are included. This can be justified by the following analysis. The pulsed-transform of a function G(s) for $s = j\omega$ can be expressed as

$$G^*(j\omega) = \frac{1}{T} \sum_{n=-\infty}^{\infty} G(j\omega + jn\omega_s) \qquad n = 0, 1, 2, \cdots$$

or

$$G^*(j\omega) = \frac{1}{T}\left[G(j\omega) + G(j\omega + j\omega s) + G(j\omega - j\omega s) + G(j\omega + 2j\omega s) + G(j\omega - 2j\omega s) + \cdots\right] \qquad (22)$$

If the system acts as a low pass filter, the higher frequency components of (22) can be assumed negligible, and $G^*(j\omega)$ can be approximated

by the first few terms of (22). If the pulse transform of (21) is approximated by the first term of (22) with the zero-order hold included, then

$$G^*(j\omega) \approx -\frac{1}{T}\left(\frac{W_{ss}G_1H_o}{1 - W_{ss}G_2}\right)(j\omega) \qquad (23)$$

The Nyquist diagram of (23) is shown as Curve B in Figure 3. The approximation used in (23) is good at low frequencies but poor at high frequencies, indicating that the terms of (22) involving the sampling frequency can not be neglected at the higher frequencies. The frequency at which Curves A and B separate is $\omega = 4$ radians per second.

IV. DETERMINATION AND ANALYSIS OF DIGITAL COMPENSATION

As explained in the previous section and shown in Curve A of Figure 3, the sampled-data system is unstable. Since the open loop system has one pole outside the unit circle in the z-plane, as shown in (17) from (18), the Nyquist plot must encircle the zero db point once in the clockwise direction in order that the system may be stable. In order to do this, gain and phase lag must be added to the system to shift the curve below the zero db point. By trial and error a suitable digital compensation was determined to be

$$D(z) = 562\left(\frac{z - 0.92}{z - 0.90}\right) \tag{24}$$

Curve B of Figure 4 is the Nyquist plot of (17) with the digital compensation added. The sampled-data system is now stable since there is one clockwise encirclement of the zero db point. The phase margin is 45° and the gain margin is 9 db. Curve A of Figure 4 is the Nyquist plot of the uncompensated sampled-data system and was included for comparison purposes.

The roots of the characteristic equation of (12) were determined on the IBM 7040 digital computer to be

$$\begin{aligned} z &= 0.3894 + j0.4565 \\ z &= 0.3894 - j0.4565 \\ z &= 0.9963 + j0 \\ z &= 0.9839 + j0 \\ z &= 0.9152 + j0 \end{aligned}$$

None of the roots lie outside the unit circle in the z-plane, indicating that the compensated system is stable and checking the Nyquist results. However, since the system is open-loop unstable with the digital compensation added, the system will be stable only at the sampling instants and will be unstable between sampling instants. Therefore this system cannot be compensated to stability by the use of digital compensation in the ϕ - path alone.

It was felt to be of interest to investigate the effects of the compensation in the continuous-data system. One method that can be used to find a continuous-data compensation equivalent to D(z) is shown in Figure 7. For this figure,

$$D(z) = H_o G_c(z) \tag{25}$$

Since $H_o = \frac{1 - z^{-1}}{s}$,

$$\mathcal{Z}\left[\frac{G_c(s)}{s}\right] = \left[\frac{1}{1 - z^{-1}}\right] D(z)$$

For the digital compensation given by (24)

$$\mathcal{Z}\left[\frac{G_c(s)}{s}\right] = \left[\frac{z}{z - 1}\right]\left[\frac{562(z - 0.99)}{z - 0.90}\right]$$

Thus

$$\frac{G_c(s)}{s} = \frac{562(s + 0.257)}{s(s + 2.57)}$$

or

$$G_c(s) = \frac{562\ (s + 0.257)}{s + 2.57} \tag{26}$$

Curve A of Figure 5 is the Nyquist diagram of (21) with the continuous-data compensation shown in (26) added. This curve neglects the effects of the zero-order hold. Curve B is the Nyquist plot of (21) without the compensation and was included here for comparison purposes. The two Nyquist plots shown in Figure 5 for the continuous-data system correlate very well with the two curves of Figure 4 for the sampled-data system in the low frequency range. The phase and gain margins of the continuous system are 45° and 9 db respectfully which correlates very well with the results obtained above for the sampled system. The roots of the characteristic equation of the continuous-data system with compensation were found to be

$$\begin{aligned} s &= -\ 0.17000187 + j0.18776354 \\ s &= -\ 0.17000187 - j0.18776354 \\ s &= -\ 12.516019 + j21.638564 \\ s &= -\ 12.516019 - j21.638564 \\ s &= -\ 2.1979575 \end{aligned}$$

All roots lie in the left halfplane, checking the Nyquist results.

Curves A and B of Figure 6 are the same as the curves of Figure 5 with the effects of the zero-order hold included and with the approximation used in (23).

V. CONCLUSIONS

The pulsed transfer function for the simplified thrust vector control system for a Saturn-type vehicle was derived. In the simplified thrust vector control system, the bending modes of the vehicle are ignored and the lateral acceleration channel is omitted. Typical data was used in an example, and the uncompensated system was unstable. A digital transfer function was chosen which compensated the system to stability at sampling instances with a gain margin of nine db and a phase margin of 45°. An equivalent continuous-data compensation was employed with the continuous-data system, resulting in the same gain and phase margins. Numerical accuracy was critical for the sampled-data case, with at least eight significant figures required in obtaining the z-transforms.

For the example, the system was unstable between sampling instances, indicating what is referred to in current literature as "hidden instability". Thus additional compensation would be required in the attitude rate channel. This problem has not been considered in this report. Also the dynamic response of the control system is not considered.

APPENDIX A

DERIVATION OF TRANSFER FUNCTION β_e^*/R^* BY THE COMPOSITE SIGNAL FLOW GRAPH METHOD

The first step in deriving the system transfer function by the composite signal flow graph method is to construct the signal flow graph of the sampled-data system. This is done by designating all junction points as nodes and showing each of the branches as arrows pointing in the direction of signal flow. The transfer function of each branch should be labeled on its arrow. Since all samplers are included in the graph, and since a transfer function cannot be written for a sampler, the system transfer function cannot be calculated as yet.

The second step is to construct the modified signal flow graph. This is done by replacing all of the samplers by pulsed input signals as shown in Figure 8. In this case the pulsed input signal is equal to the pulsed output of node X_1. From the modified signal flow graph the signal at each node as a function of the system inputs can be obtained by using Mason's gain formula, which states that

$$X = \sum_K \frac{M_K \Delta_K}{\Delta} \tag{27}$$

where X is the value of the signal at the node, M_K is the gain of the Kth forward path, Δ = 1 - (sum of all individual loop gains) + (sum of gain products of all possible combinations of two nontouching loops) - (sum of the gain products of all possible combinations of three nontouching loops) + ..., and Δ_K is that value of Δ evaluated for all paths not touching the Kth forward path[2].

Applying Masons' gain formula to Figure 8, the following is obtained:

$$X_1 = \left[\frac{R(1 - G_2W_{ss})}{1 - G_2W_{ss}}\right] + \left[\frac{H_oG_1W_{ss}}{1 - G_2W_{ss}}\right] D^* X_1^*$$

$$X_2 = X_1^*$$

$$X_3 = \left[\frac{H_o}{1 - G_2W_{ss}}\right] D^* X_1^* \qquad (28)$$

$$X_4 = \left[\frac{H_oW_{ss}}{1 - G_2W_{ss}}\right] D^* X_1^*$$

The pulse transform of (28) is

$$X_1^* = R^* + \left(\frac{H_oG_1W_{ss}}{1 - G_2W_{ss}}\right)^* D^* X_1^*$$

$$X_2^* = X_1^*$$

$$X_3^* = \left(\frac{H_o}{1 - G_2W_{ss}}\right)^* D^* X_1^* \qquad (29)$$

$$X_4^* = \left(\frac{H_oW_{ss}}{1 - G_2W_{ss}}\right)^* D^* X_1^*$$

Care must be taken in obtaining (29) since the pulse transform of a product is not equal to the product of the pulse-transformed functions. Therefore all nonsampled functions must be grouped before the pulse transform is taken.

The next step is to construct the sampled signal flow graph from the results obtained above. This is done by indicating the pulsed nodes on the graph and constructing the branches as dictated by (29). The results are shown in Figure 9.

The composite signal flow graph shown in Figure 10 can now be constructed using Figures 8 and 9 by obtaining the artificial sampler inputs for the modified signal flow graph from the sampled signal flow graph. The pulsed system transfer function and the continuous output transfer function can now be obtained by using Mason's gain formula.

$$\frac{C_e^*}{R^*} = \frac{\left(\frac{H_oW_{ss}}{1 - G_2W_{ss}}\right)^* D^*}{1 - \left(\frac{H_oG_1W_{ss}}{1 - G_2W_{ss}}\right)^* D^*} \qquad (30)$$

$$\frac{C_e}{R^*} = \frac{\left(\frac{H_o W_{ss}}{1 - G_2 W_{ss}}\right) D^*}{1 - \left(\frac{H_o G_1 W_{ss}}{1 - G_2 W_{ss}}\right)^* D^*} \tag{31}$$

At first glance this method of deriving a system transfer function seems more tedious than working through the system and solving simultaneous equations. However, one familiar with the techniques and with Mason's gain formula can perform the above steps by inspection. Of course, this method is better suited to complex, multi-loop systems than to simple systems, because of the time-saving factor. Figure 10 need not be drawn separately if Figures 8 and 9 are drawn so that they may be readily connected. Equations (29) may be obtained directly from Figure 8 by writing (28) and taking the pulse transform at the same time.

In summary, the system transfer function may be obtained by constructing the modified signal flow graph, writing the pulse-transformed node equations and constructing the sampled signal flow graph from these equations, connecting the two graphs, and then obtaining the transfer function directly by using Mason's gain formula.

APPENDIX B

METHODS OF ANALYSIS OF A FUNCTIONAL RELATIONSHIP CONTAINING s AND ε^{sT}

Consider the function

$$\beta_e = \frac{\left(\frac{W_{ss}H_o}{1 - W_{ss}G_2}\right)}{1 - \left(\frac{W_{ss}G_1H_o}{1 - W_{ss}G_2}\right)^*} R^* \tag{32}$$

Rewriting the equation

$$\beta_e = \left[\frac{W_{ss}H_o}{1 - W_{ss}G_2}\right]\left[\frac{1}{1 - \left(\frac{W_{ss}G_1H_o}{1 - W_{ss}G_2}\right)^*}\right]\left[R^*\right] = \tag{33}$$

$$F_1(s)\, F_2(\varepsilon^{sT})\, F_3(\varepsilon^{sT})$$

If R(s) is the Laplace transform of a bounded function, then $\beta_e(t)$ is bounded if the poles of

$$\frac{\beta_e}{R^*} = F_1(s)\, F_2(\varepsilon^{sT}) \tag{34}$$

do not lie in the right halfplane. The factors $F_1(s)$ and $F_2(\varepsilon^{sT})$ can be examined jointly or separately.

Consider separate investigation first. The stability contribution of $F_1(s)$ is determined by the poles of

$$F_1(s) = \frac{W_{ss} H_o}{1 - W_{ss}G_2} \tag{35}$$

It should be noted that H_o contains an ε^{sT} factor, i.e.,

$$H_o = \frac{1 - \varepsilon^{-sT}}{s} \tag{36}$$

However, this factor will not affect the poles of (35) that occur in the right halfplane. Thus the stability contribution of (35) can be examined by use of a Nyquist diagram of $\left[-W_{ss}G_2\right]$.

The stability contribution of $F_2(\varepsilon^{sT})$ is determined by the poles

$$F_2(s) = \frac{1}{1 - \left(\frac{W_{ss}G_1H_o}{1 - W_{ss}G_2}\right)^*} \tag{37}$$

This stability contribution can be examined by use of a Nyquist diagram of

$$- \left(\frac{W_{ss}G_1H_o}{1 - W_{ss}G_2}\right)^* \tag{38}$$

This function is periodic in ω, and need be examined only for that part of the Nyquist path along the $j\omega$ axis, $-\frac{\omega_s}{2} \leq \omega \leq \frac{\omega_s}{2}$, where $\omega_s = 2\pi f_s$, and

f_s is the sampling frequency. Since the function is periodic in ω, the Nyquist diagram for that part of the path $(n - \frac{1}{2})\omega_s \leq \omega \leq (n + \frac{1}{2})\omega_s$, $n = 1, 2, \ldots$, is congruent with the diagram obtained for $-\frac{\omega_s}{2} \leq \omega \leq \frac{\omega_s}{2}$. In fact, the Nyquist diagram need be constructed only for the path $0 \leq \omega \leq \frac{\omega_s}{2}$, since the diagram for the path $-\frac{\omega_s}{2} \leq \omega \leq 0$ is the complex conjugate of the diagram for the path $0 \leq \omega \leq \frac{\omega_s}{2}$.

If the two functions, F_1 and F_2, are to be investigated jointly, one method that can be used is to rewrite (32) as

$$\frac{\beta_2}{R^*} = \frac{W_{ss}H_o}{1 - W_{ss}G_2 - \left(\frac{W_{ss}G_1H_o}{1 - W_{ss}G_2}\right)^* + W_{ss}G_2\left(\frac{W_{ss}G_1H_o}{1 - W_{ss}G_2}\right)^*} \tag{39}$$

The Nyquist diagram of

$$- W_{ss}G_2 - \left(\frac{W_{ss}G_1H_o}{1 - W_{ss}G_2}\right)^* + W_{ss}G_2\left(\frac{W_{ss}G_1H_o}{1 - W_{ss}G_2}\right)^* \tag{40}$$

can be plotted for the path $0 \leq \omega \leq \infty$. The function (40) is not periodic in ω, and therefore the Nyquist path must include the entire $j\omega$ axis. This Nyquist diagram indicates the location of zeros of the function

$$(1 - W_{ss}G_2)\left[1 - \left(\frac{W_{ss}G_1H_o}{1 - W_{ss}G_2}\right)^*\right] \tag{41}$$

in the right halfplane. If the function

$$\left[1 - \left(\frac{W_{ss}G_1H_o}{1 - W_{ss}G_2}\right)^*\right] \tag{42}$$

has a zero at $s = \sigma_1 + j\omega_1$, it also has zeros at $s = \sigma_1 \pm j(\omega_1 + n\omega_s)$, $n = 1, 2, 3, \cdots$, since it is periodic in ω. Thus, if this function has one zero in the right halfplane, it has an infinity of zeros there. This will result in an infinity of enclosures of the (-1) point on the Nyquist diagram. However, these enclosurers are not congruent as in the case of the Nyquist diagram of (38), since the term $(1 - W_{ss}G_2)$ of (41) is not periodic in ω. It is felt that this method does not offer many possibilities.

Consider again (32), (38), and (41). Each zero of $(1 - W_{ss}G_2)$ is a pole of

$$\frac{W_{ss}G_1H_o}{1 - W_{ss}G_2} \tag{43}$$

From sampled-data theory[3], if (43) has a pole at $s = \sigma_1 + j\omega_1$, then

(38) has poles at $s = \sigma_1 \pm j(\omega_1 + n\omega_s)$, $n = 0, 1, 2, \cdots$, except for a case that is mentioned in the next paragraph. Therefore the zeros of $(1 - W_{ss}G_2)$ will be cancelled by poles of (38), and $(1 - W_{ss}G_2)$ need not be considered in the stability investigation. If the sampled transform of (32) is taken, then

$$\frac{P_e^*}{R^*} = \frac{\left(\frac{W_{ss}H_o}{1 - W_{ss}G_2}\right)^*}{1 - \left(\frac{W_{ss}G_1H_o}{1 - W_{ss}G_2}\right)^*} \tag{44}$$

The stability of the system can then be determined from (38), and the analysis may be made either in the s-plane or in the z-plane. The Nyquist diagram will be identical in each case.

It is possible that, when the pulse transform of (43) is taken, certain roots of the denominator will be cancelled by the appearance of these roots in the numerator[4]. This case can occur only if the imaginary part of the root is equal to $n\omega_s/2$, $n = 1, 2, 3, \cdots$. For this case, investigation of (44) will not indicate the presence of these poles in (43). If these cancelled roots are unstable, the system will be unstable between sampling instances, and this instability will not be indicated by an investigation of (44). Also, if (43) has complex poles in the left halfplane for which the imaginary part is greater than $\omega_s/2$, the response between sampling instances can be oscillatory. The oscillations are referred to in the literature as "hidden oscillations". One method that can be used to determine the nature of the response between sampling instances is to examine the roots of (43). Another method is to examine

the modified z-transform of (43). The modified z-transform method appears to be the more popular method at the present time. In summary, if (43) has complex poles for which the imaginary part is equal to or greater than $\omega_s/2$, the system response between sampling instances may be oscillatory, or even unstable, and no indication is given by an analysis of the pulsed-transforms.

In conclusion, if, for any pole of (43), the imaginary part is equal to or greater than $\omega_s/2$, the response of the system may not be well-behaved between sampling instances. Then an investigation of (44) is not sufficient to determine stability or transient response. Otherwise, the response between sampling instances follows the response at sampling instances, and an investigation of (44) is sufficient.

DIGITAL COMPUTER PROGRAM AND SAMPLE OUTPUT DATA

```
C  NYQUIST PLOTS OF S R Z PLANES
C     K=1   R AND S PLANES, K=2 Z PLANE
      DIMENSION A(25,2), B(25,2)
   10 FORMAT(4X,3I2,E15.8)
   20 FORMAT(4X,2E15.8)
   30 FORMAT(19HERROR IN INPUT DATA)
   40 FORMAT(///,95H                                   MAGNITUD
     1E        MAGNITUDE   DB          RADIANS          ANGLE       CYCLES
     /)
   50 FORMAT (4X,F15.8,4X,F15.8,4X,F15.8,4X,F15.8,4X,F15.8)
   60 FORMAT(///,4X,18H K M N     CONSTANT,/)
   90 READ 10, K,M,N,C
      PRINT 60
      PRINT 10, K,M,N,C
      W=C.C
      DEG=0.0
      T=0.04
      AN=1.0
      RN=1.0
      AG=0.0
      RG=0.0
      IF (N) 3,20,19
   19 DO 11 I=1,N
      READ 20, A(I,1),A(I,2)
   11 PRINT 20, A(I,1),A(I,2)
   20 DO 12 I=1,M
      READ 20, B(I,1),B(I,2)
   12 PRINT 20, B(I,1),B(I,2)
      PRINT 40
   96 IF (K-1) 3,83,84
   84 IF(175.0-DEG) 99,98,98
   98 DEG=DEG+5.0
      W=(DEG*3.14159)/180.0
      WS=SIN(W)
```

```
      WC=COS(W)
      GO TO 25
   82 IF (3.00-W) 99,97,97
   97 W=W+0.01
      WS=W
      WC=0.0
   25 IF (N) 3,15,16
   16 AN=1.0
      AG=0.0
      DO 13 I=1,N
      AN=AN*SQRT((WS+A(I,2))**2+(WC+A(I,1))**2)
      IF(((A(I,1)+WC).EQ.0.0).OR.((ABS((A(I,2)+WS)/(A(I,1)+WC))).GT.1.0E+2
     1)).AND.(A(I,2)+WS).GT.0.0) AG=AG+3.14159
      IF((A(I,1)+WC).LT.0.0)AG=AG+3.14159+ATAN((WS+A(I,2))/(WC+A(I,1)))
      IF((A(I,1)+WC).GT.0.0)                AG=AG+ATAN((WS+A(I,2))/(WC+A(I,1)))
      GO TO 13
   87 AG=AG-(3.1416/2.0)
      GO TO 13
   88 GO TO 3
   89 AG=AG+(3.1416/2.0)
   13 CONTINUE
   15 BN=1.0
      BG=0.0
      DO 14 I=1,M
      BN=BN*SQRT((WS+B(I,2))**2+(WC+B(I,1))**2)
      IF(((B(I,1)+WC).EQ.0.0).OR.((ABS((B(I,2)+WS)/(B(I,1)+WC))).GT.1.0E+2
     1)).AND.(B(I,2)+WS).GT.0.0) BG=BG+3.14159
      IF((B(I,1)+WC).LT.0.0)BG=BG+3.14159+ATAN((WS+B(I,2))/(WC+B(I,1)))
      IF((B(I,1)+WC).GT.0.0)                BG=BG+ATAN((WS+B(I,2))/(WC+B(I,1)))
      GO TO 14
   77 BG=BG-(3.1416/2.0)
      GO TO 14
   78 GO TO 3
```

DIGITAL COMPUTER PROGRAM
(CONCLUDED)

```
 79 BG=BG+(3.1416/2.0)
 14 CONTINUE
    AHOLD=0.0
    HOLD=1.0
 58 AMAG=ABS(C)*(AN/RN)*HOLD
    AMDR=20.0*ALOG10(AMAG)
    ANG=AG-BG+AHOLD
    IF (C) 2,3,4
  2 CG=180.0
    GO TO 5
  4 CG=0.0
    GO TO 5
  5 ANGLE=CG+(ANG*180.0)/(3.14159)
    F=W/(2.0*3.14159)
 33 PRINT 50, W, AMAG, AMDR, ANGLE
    GO TO 96
  3 PRINT 30
    GO TO 99
    END
```

K M N CONSTANT

2 5 4 0.65416809E-02

INPUT DATA

.99000000E 00 0.
.61289024E 00 0.
.11527473E 01-0.53606735E 00
.11527473E 01 0.53606735E 00
.39296640E-00 0.46203788E-00
.39296640E-00-0.46203788E-00
.10068908E 01 0.
.99309661E 00 0.
.90000000E 00 0.

RADIANS	MAGNITUDE	[illegible]	ANGLE
.87266388E-01	0.11918125E-00	-0.18475842E 02	0.21602522E 03
.17453278E-00	0.40409939E-01	-0.27870237E 02	0.19017451E 03
.26179916E-00	0.19929502E-01	-0.34010071E 02	0.16812353E 03
.34906555E-00	0.12319720E-01	-0.38187983E 02	0.14386110E 03
.43633194E-00	0.93343242E-02	-0.40598342E 02	0.11594474E 03
.52359833E 00	0.85862313E-02	-0.41323948E 02	0.87428396E 02
.61086471E 00	0.89794869E-02	-0.40934969E 02	0.61810077E 02
.69813111E 00	0.98592151E-02	-0.40123153E 02	0.39582806E 02
.78539749E 00	0.10817882E-01	-0.39317156E 02	0.19766321E 02
.87266388E 00	0.11590108E-01	-0.38718250E 02	0.16149040E 01
.95993027E 00	0.12027975E-01	-0.38396150E 02	-0.15084923E 02
.10471967E 01	0.12105942E-01	-0.38340028E 02	-0.30264927E 02
.11344630E 01	0.11892271E-01	-0.38494704E 02	-0.43850671E 02

.12217294E 01	0.11491415E-01	-0.38792530E 02	-0.55883616E 02
.13089958E 01	0.10997665E-01	-0.39173990E 02	-0.66514275E 02
.13962622E 01	0.10477169E-01	-0.39595120E 02	-0.75943625E 02
.14835286E 01	0.99692392E-02	-0.40026760E 02	-0.84376690E 02
.15707950E 01	0.94940959E-02	-0.40450928E 02	-0.91997171E 02
.16580614E 01	0.90602502E-02	-0.40857196E 02	-0.98959237E 02
.17453278E 01	0.86696990E-02	-0.41239920E 02	-0.10538789E 03
.18325941E 01	0.83211167E-02	-0.41596368E 02	-0.11138316E 03
.19198605E 01	0.80116770E-02	-0.41925531E 02	-0.11702458E 03
.20071269E 01	0.77380348E-02	-0.42227386E 02	-0.12237558E 03
.20943933E 01	0.74968321E-02	-0.42502445E 02	-0.12748702E 03
.21816597E 01	0.72849366E-02	-0.42751485E 02	-0.13239996E 03
.22689261E 01	0.70995433E-02	-0.42975392E 02	-0.13714795E 03
.23561925E 01	0.69382003E-02	-0.43175064E 02	-0.14175863E 03
.24434589E 01	0.67987991E-02	-0.43351356E 02	-0.14625511E 03
.25307252E 01	0.66795505E-02	-0.43505056E 02	-0.15065685E 03
.26179917E 01	0.65789558E-02	-0.43636861E 02	-0.15498058E 03
.27052580E 01	0.64957781E-02	-0.43747376E 02	-0.15924081E 03
.27925244E 01	0.64290137E-02	-0.43837113E 02	-0.16345037E 03
.28797908E 01	0.63778726E-02	-0.43906484E 02	-0.16762082E 03
.29670572E 01	0.63417575E-02	-0.43955808E 02	-0.17176269E 03
.30543236E 01	0.63202519E-02	-0.43985312E 02	-0.17588589E 03
.31415900E 01	0.63131104E-02	-0.43995133E 02	-0.17999986E 03

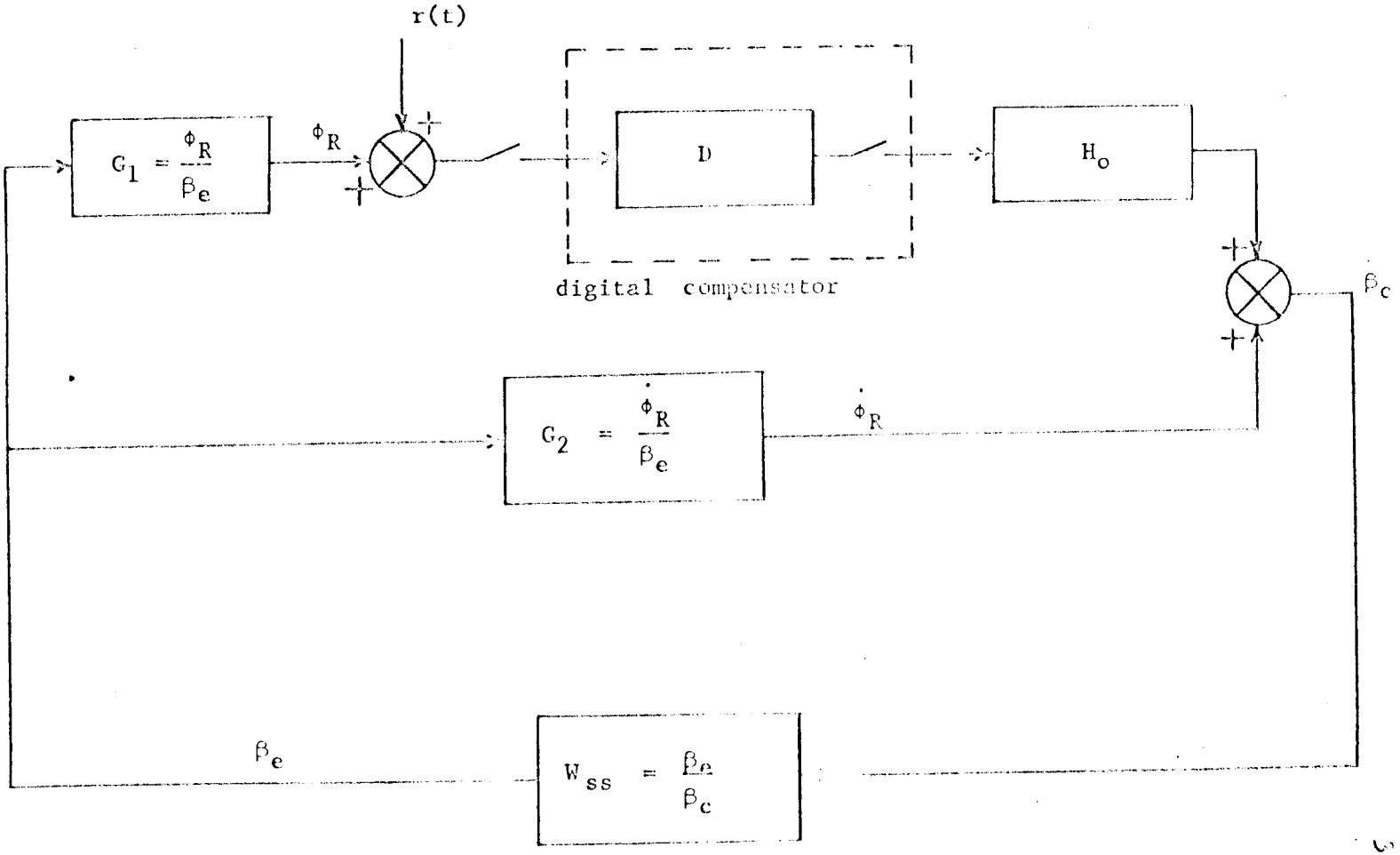

Figure 1. THE SIMPLIFIED THRUST VECTOR CONTROL SYSTEM WITH DIGITAL COMPENSATION

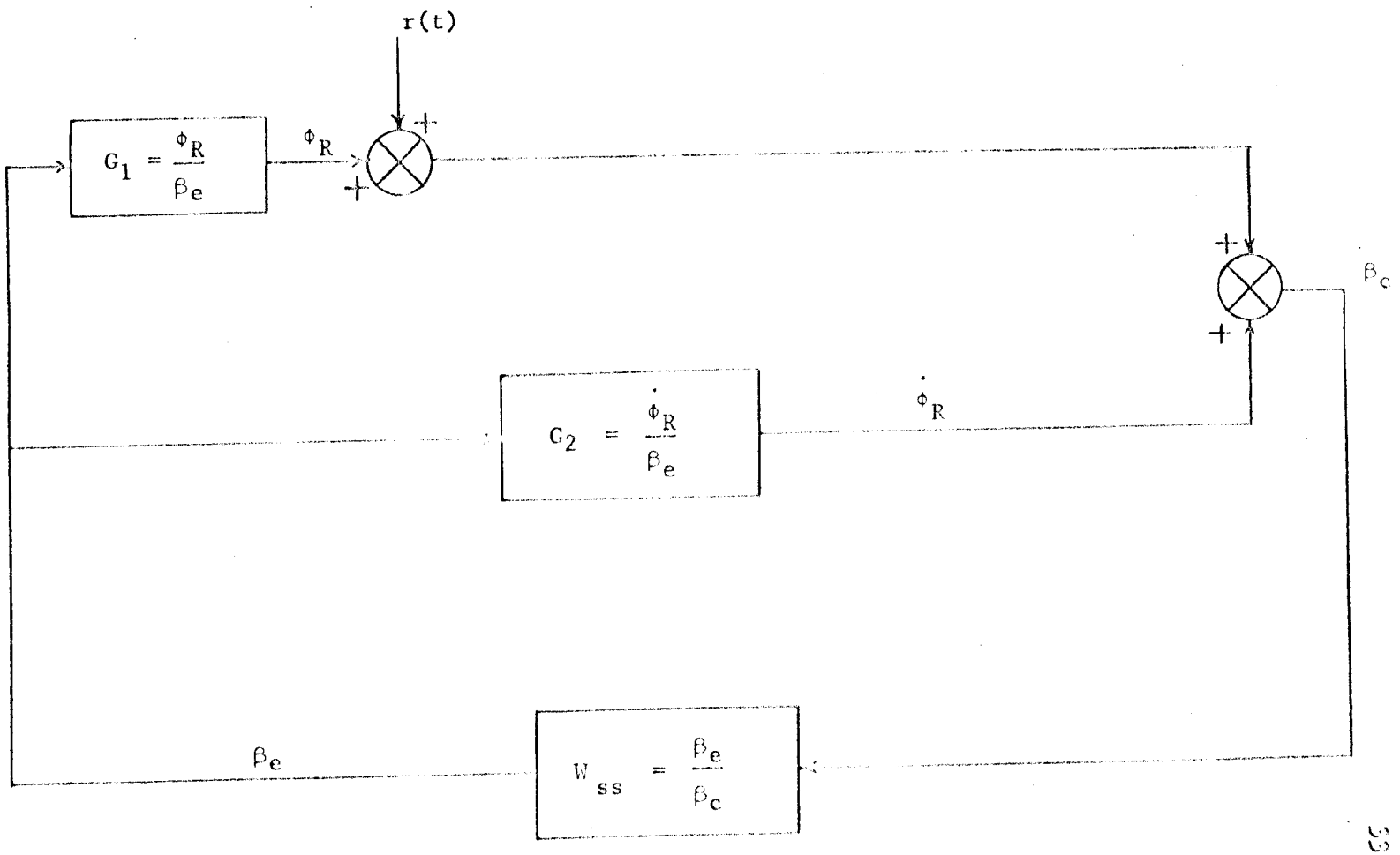

Figure 2. THE SIMPLIFIED THRUST VECTOR CONTROL SYSTEM

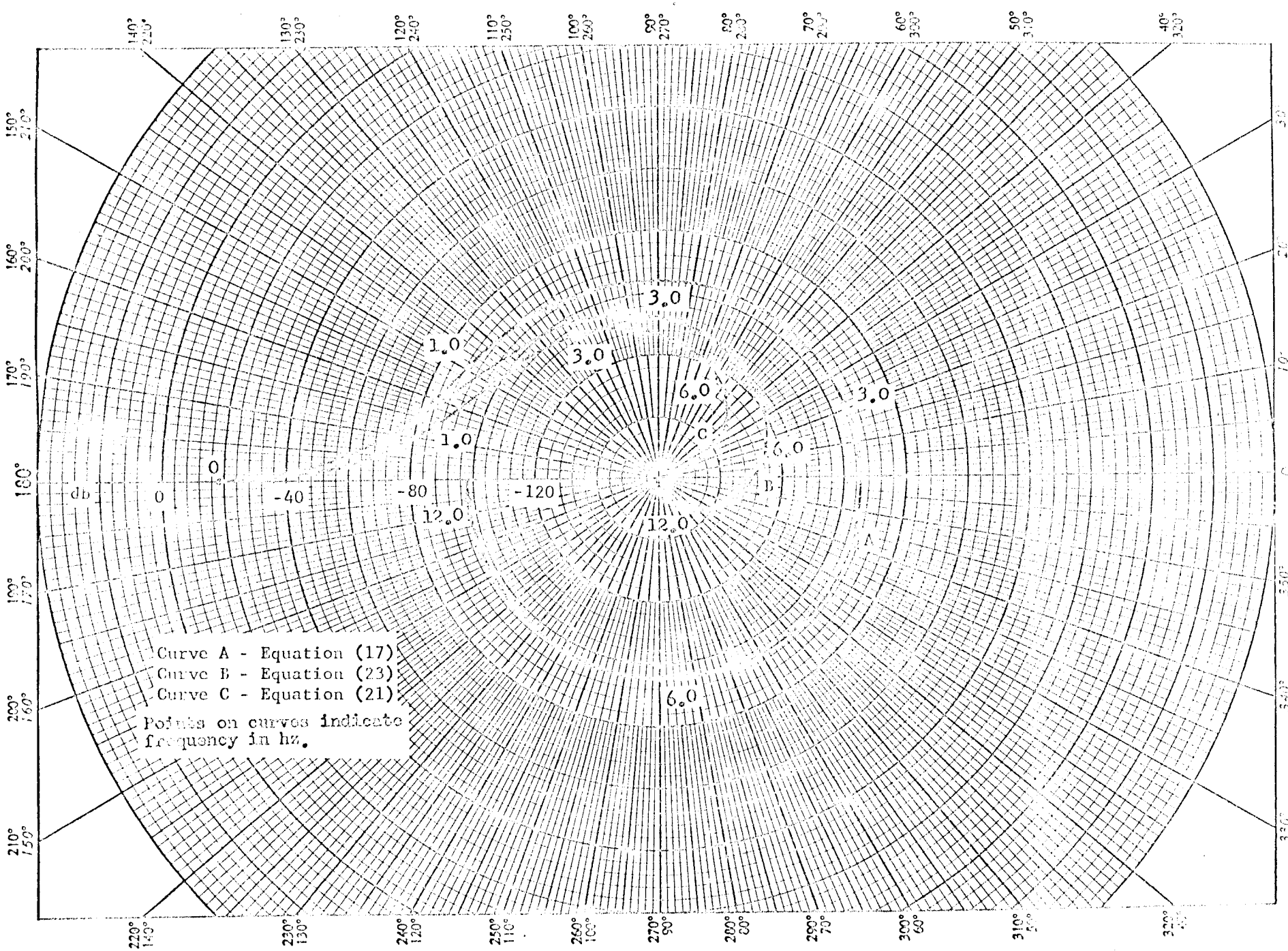

Figure 3. NYQUIST DIAGRAMS FOR UNCOMPENSATED SYSTEMS

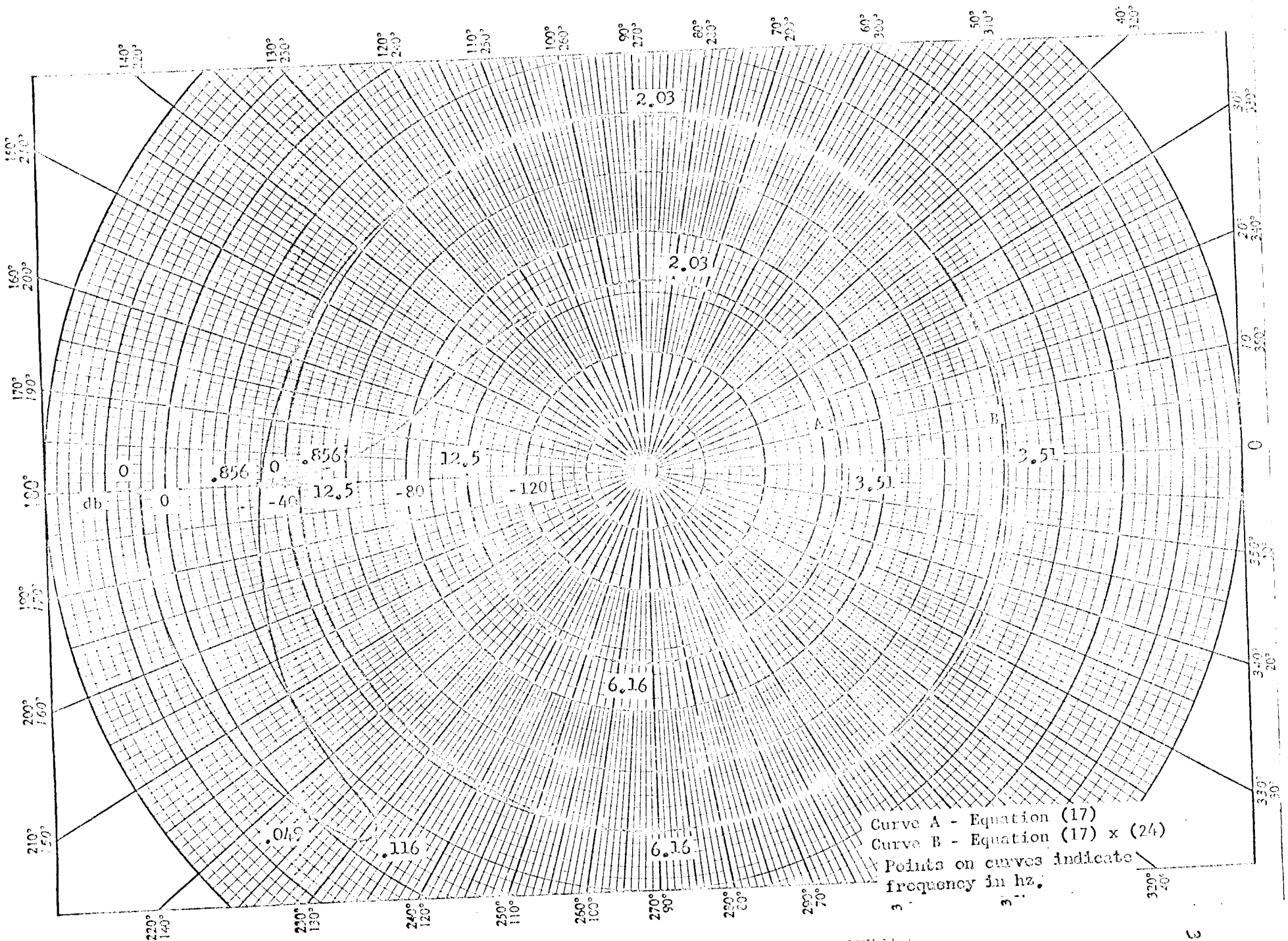

Figure 4. NYQUIST DIAGRAMS FOR SAMPLED-DATA SYSTEMS

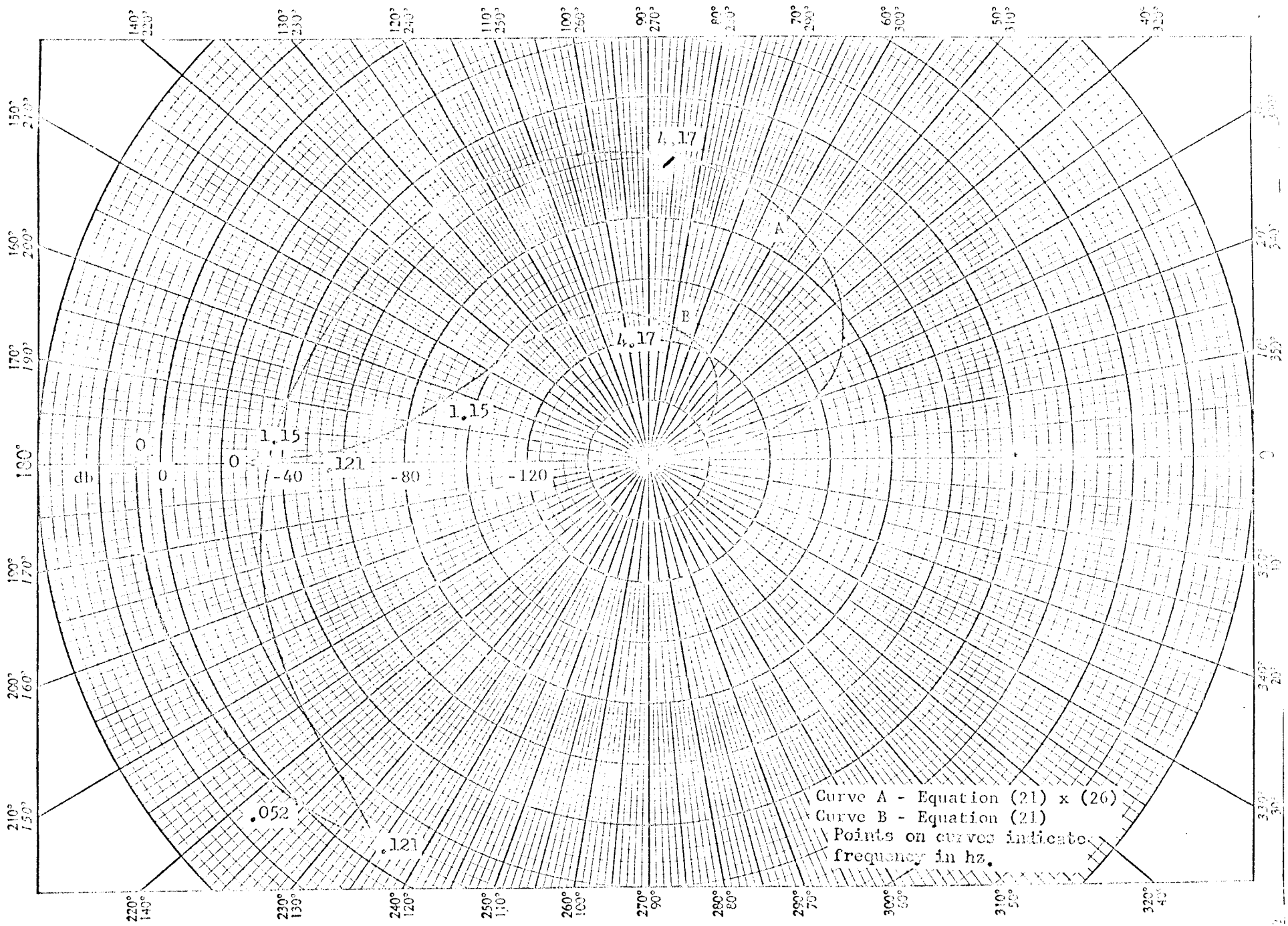

Figure 5. NYQUIST DIAGRAMS FOR CONTINUOUS-DATA SYSTEMS

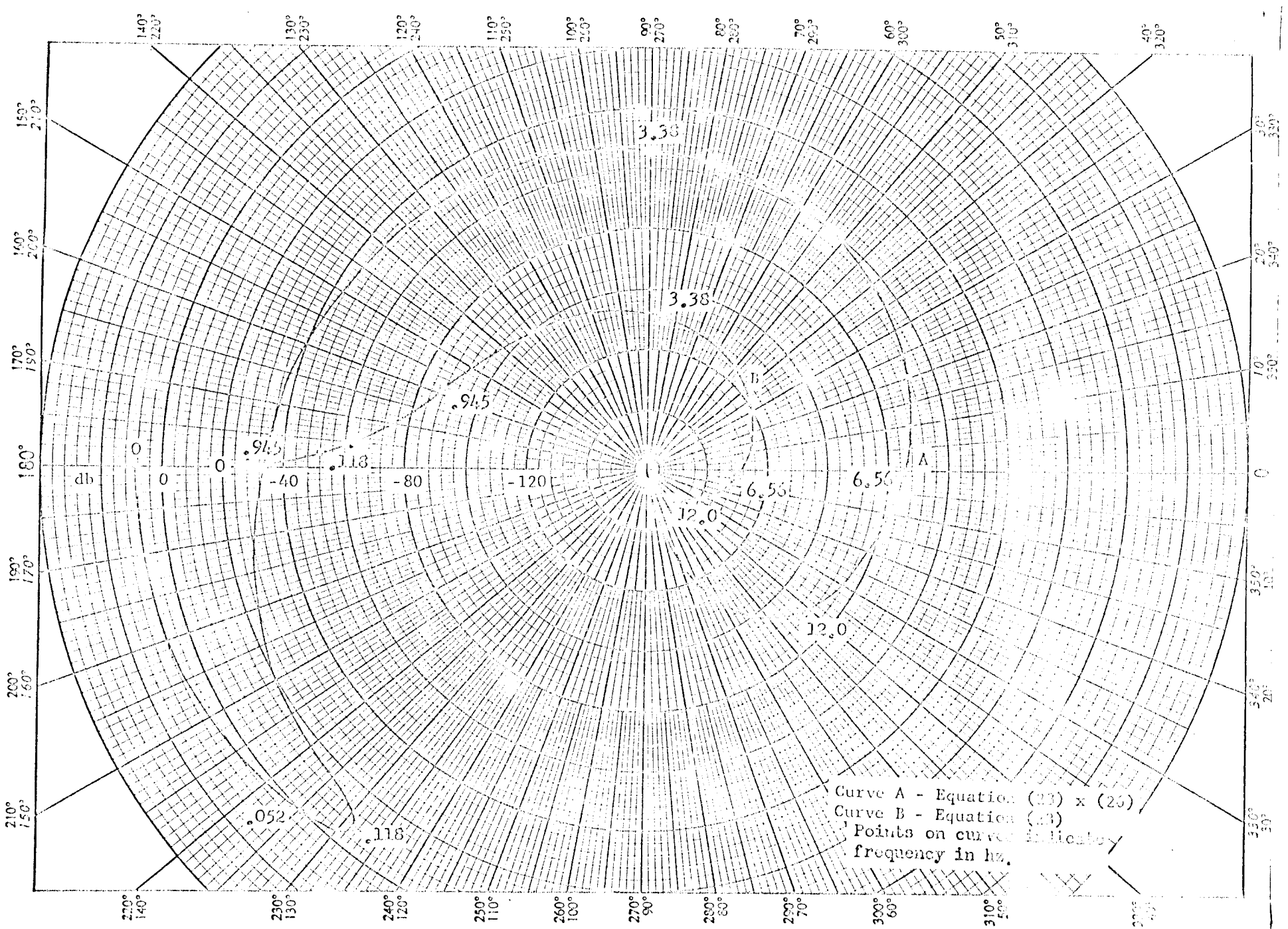

Figure 6. NYQUIST DIAGRAMS FOR PULSED-TRANSFORM APPROXIMATIONS

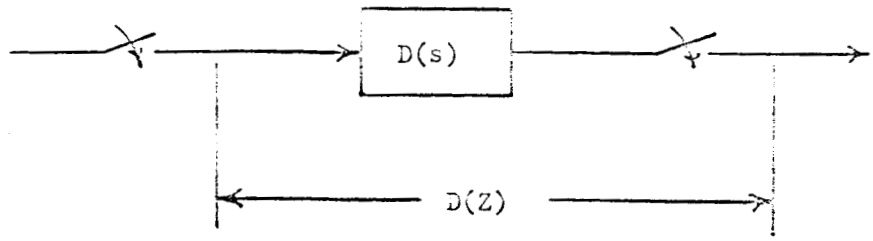

(a) Digital Controller

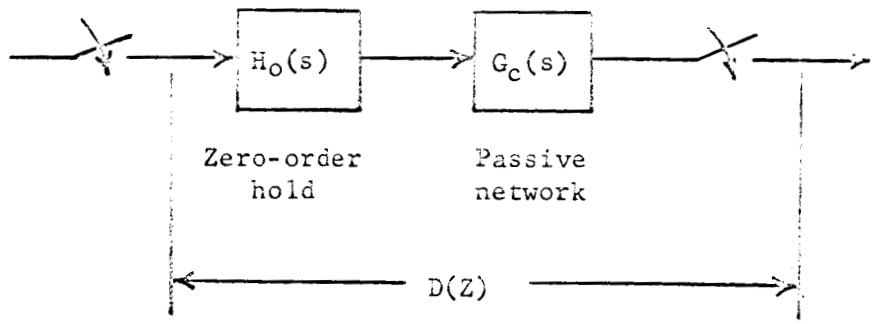

(b) Equivalent Series Pulse-data Network

Figure 7. EQUIVALENT SERIES PULSE-DATA NETWORK FOR DIGITAL COMPENSATION

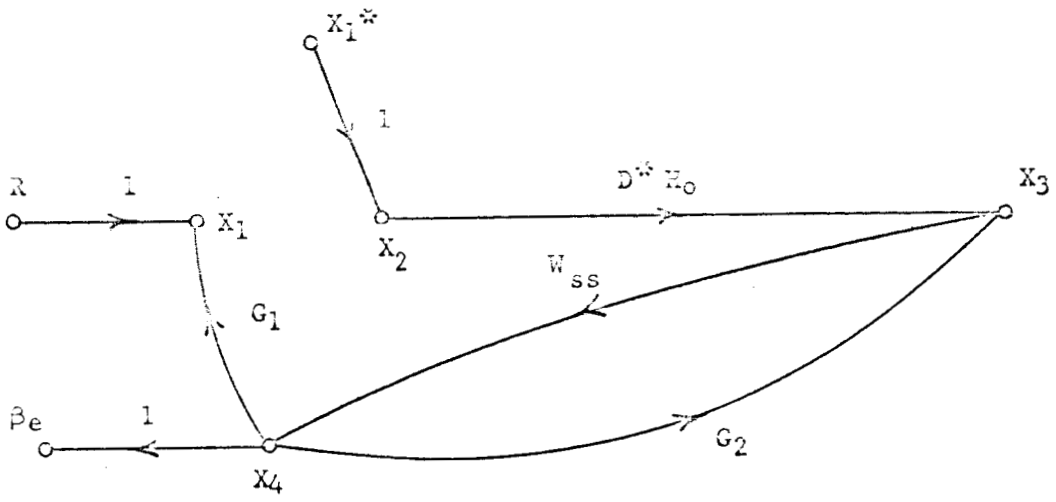

Figure 8 . MODIFIED SIGNAL FLOW GRAPH

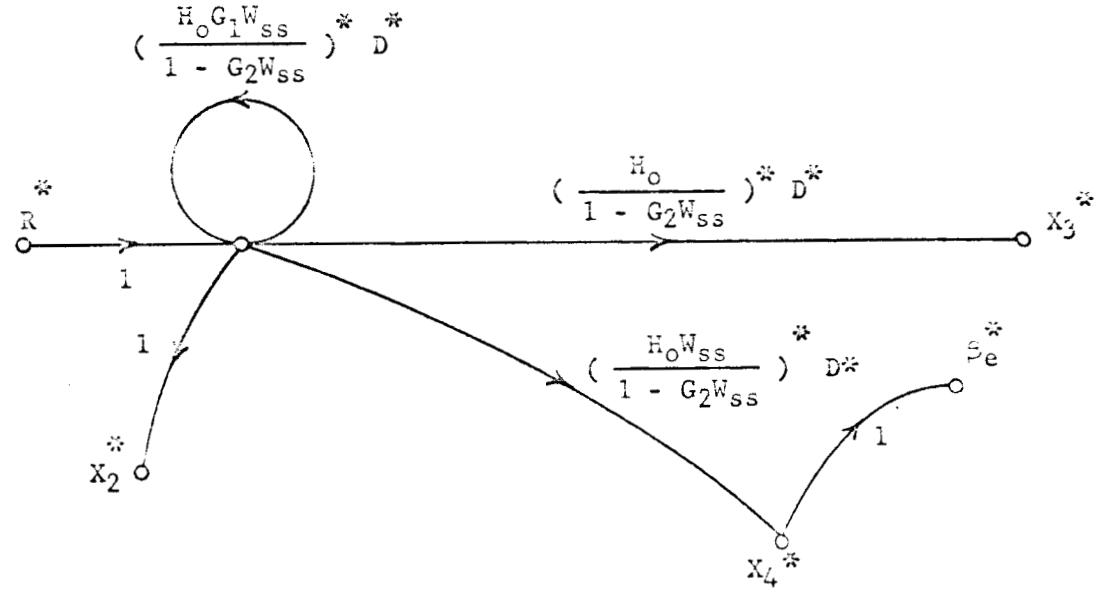

Figure 9 . SAMPLED SIGNAL FLOW GRAPH

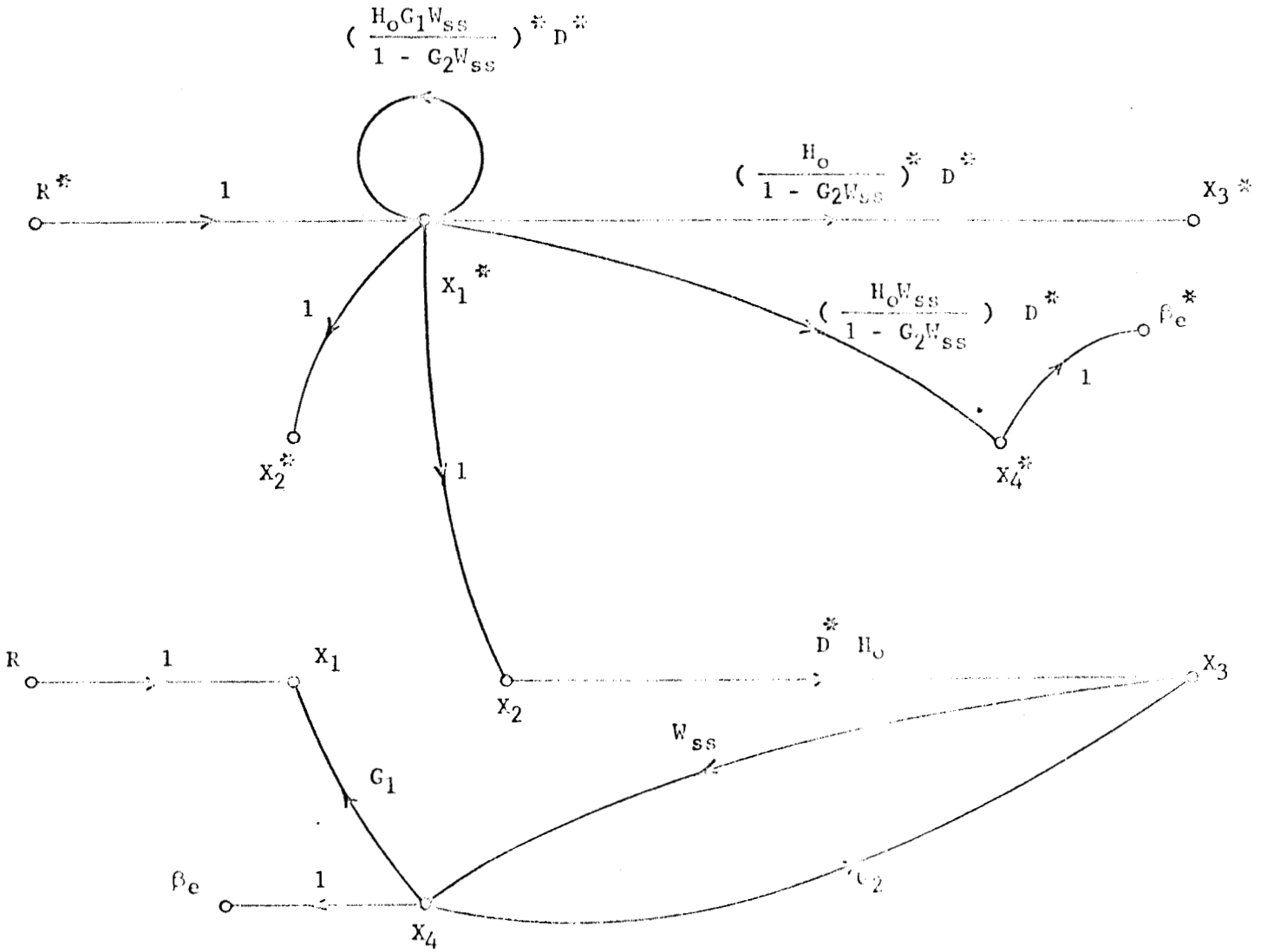

Figure 10 . COMPOSITE SIGNAL FLOW GRAPH

REFERENCES

1. B. C. Kuo, Analysis and Synthesis of Sampled-Data Control Systems, Prentice-Hall, Inc., Englewood Cliffs, N. J., pp. 275-276; 1963

2. S. J. Mason, "Feedback theory- further properties of signal flow graphs," Proc. IRE, vol. 44, pp. 920-926; July, 1956.

3. B. C. Kuo, Analysis and Synthesis of Sampled-Data Control Systems, Prentice-Hall, Inc. Englewood Cliffs, N. J., p. 37; 1963.

4. E. I. Jury, "Hidden oscillations in sampled-data control systems," AIEE Trans., vol. 75, pt. II, pp. 391-395; January, 1957.